UNITED STATES DEPARTMENT OF THE INTERIOR

GEOLOGICAL SURVEY

Colored Gravity Anomaly and Terrain Maps of the East Central United States

by

R. W. Simpson and R. H. Godson

Open-File Report 81-846

1981

Colored Gravity Anomaly and Terrain Maps of the East Central United States

by

R. W. Simpson and R. H. Godson

INTRODUCTION

We have plotted the gravity and terrain data available to us for the East Central portion of the United States. Colored maps displaying this data are provided as 5" x 7" color Xeroxes with this report. Standard 2" x 2" color slides of these maps are available through the U.S. Geological Survey Photo Library (Mail Stop 914, Box 25046, Denver Federal Center, Denver, CO 80225, telephone 303/234-4004). These maps are similar in scale and content to another set prepared for the Northeastern United States (Simpson and others, 1981).

The distribution of anomalies, when compared with patterns of seismicity, may provide some clues as to the origin of intraplate seismicity in the Eastern U.S. For example, earthquakes do not seem to occur very frequently in areas with low gravity gradients, while areas with moderate to high amplitude residual anomalies sometimes (though not always) have concentrations of seismicity nearby. There is a hint that regions with a northeast grain to the residual anomalies experience more earthquakes than areas with other trends or with random patterns of anomalies.

THE DATA SETS

1. Gravity Data

The gravity data were extracted from the Department of Defense (DOD) gravity data set available through the National Oceanic and Atmospheric Administration (NOAA) Data Center. (NOAA, National Geophysical and Solar-Terrestrial Data Center, Boulder, CO 80302). Additional data from the Coastal Plain of South Carolina collected by Alan Cogsbill were supplied by the Geothermal Program at Virginia Polytechnic Institute.

Because of time limitations, the basic data set was not edited at all, but was screened to extract only one station for every 6x6 km cell (Figure 1) in order to obtain a more uniform density of data points. Not surprisingly, a dozen or more bad values have crept into the data set and these are especially apparent in the gradient and derivative maps where they show up as small four-petal flower patterns. Questions about single small anomalies should always be referred to larger scale maps and to the original published maps where possible. We are confident that the major anomalies and trends are real and the excellent correspondence of many smaller anomalies with mapped geologic units suggests that most of the smaller anomalies are real.

A minimum curvature algorithm (Briggs, 1974), programmed by Webring (1977), was then used to do the necessary interpolation and extrapolation to produce a grid of values with 5 km interval between grid points.

The original grid was approximately 70 km larger on all sides, and was trimmed to the size displayed in the maps in order to reduce edge effects. Possible edge effects in the form of linear anomalies paralleling the edges of the map still appear on certain of the maps, however, and the user should be aware of this problem.

The final step was to regrid (using a splining algorithm) the basic 5 km grid to a finer 2.032 km grid size so as to be compatible with the pixel size required by the Applicon Color Plotter. White areas on the maps indicate that there were no data points within 10 km of the grid point.

The data were projected using the Albers Conic Equal-Area projection with standard parallels for the U.S. (29.5°N, 45.5°N), so that the maps are compatible with the U.S. Geologic Map.

2. Terrain Data

Terrain data were obtained from the National Geodetic Survey (NGS) who in turn received it from the Electromagnetic Compatability Analysis Center (ECAC), an agency of the Department of Defense (DOD). The data were extensively edited and reformatted (by R. H. Godson) to produce average elevations for the entire country at 30", 1', and 3' intervals. This data set has been submitted to the NOAA Data Center (National Geophysical and Solar-Terrestrial Data Center, National Oceanic and Atmospheric Administration, Boulder, CO 80303) for distribution.

DESCRIPTION OF THE MAPS

1. Free Air Gravity

This map displays the free air anomaly field calculated using the 1967 Geodetic Reference System formula for theoretical gravity (International Association of Geodesy, 1971). Observed gravity values have been adjusted to conform to the International Gravity Standardization Net of 1971 (Morelli, 1974).

2. Bouguer Gravity

Bouguer anomalies were also calculated using the new geodetic reference system (see references above) and a reduction density of 2.67 g/cm^3. Land stations in the U.S. have been computer terrain corrected into a distance of 0.895 km from the station. Estimated error on most land stations is less than about 2 milligals.

3. Bouguer Residual (250 km)

Using a Fourier transform filtering program written by Hildenbrand (1979), wavelengths greater than 250 km in the Bouguer anomaly field were suppressed. (A ramped high pass filter was used with a ramp betwen 200 km and 300 km.) This has the effect of removing a regional field consisting of the broader features of the gravity field. The regional extracted is displayed in Figure 2.

Wavelength filtering tends to produce small spurious anomalies flanking real anomalies (Ulrych, 1968). A linear high will be flanked by two small parallel lows outboard of which will be two parallel highs (of much smaller amplitude than the original). This tends to give the map a grain roughly equal in wavelength to the cut of the filter. Thus all anomalies must be interpreted with care. The dangers, we feel, are more than compensated for by the enhancement of many structures and features of geologic interest.

4. Bouguer Residual (100 km)

This map is like the last except that now wavelengths greater than 100 km have been suppressed. (A ramped high pass filter with a ramp from 80 to 120 km was used.) The regional extracted is displayed in Figure 3. Anomalies produced by a point source at 33 km depth have a half-width of 50 km. This is approximately one half of a wavelength. Thus most of the anomalies displayed in the 100 km residual map will be produced by sources at depth less than 33 km. Note, however, that not all the anomalies produced by near-surface sources have escaped the filtering; broader anomalies produced by facies changes or the gradual feathering of density contrasts over distances greater than 100 km will also be surpressed, even though the density contrast may be very near the surface.

A 100 km anomaly grain produced by the wavelength filtering is quite obvious in this map. The same caution mentioned for the 250 km residual applies here. The reality of features of interest can often be verified by comparing with the second vertical derivative which is a much smoother form of high pass filtering which does not introduce an anomaly grain at the cutoff wavelength.

Areas with low amplitude residual anomalies seem in general to have fewer earthquakes. Not all areas with high amplitude anomalies have concentrations of earthquakes, though areas with a northeast grain to the residual anomalies seem more prone to seismicity than areas with other trends. This suggests that perhaps old northeast-trending structures are being reactivated in a regional EW compressive stress field (Zoback and Zoback, 1980).

5. First Vertical Derivative of Bouguer Anomalies

The first vertical derivative of the Bouguer anomaly field was calculated using Hildenbrand's Fourier transform filtering program. The effect of this filter is to multiply the amplitude of the various wavelength components of the Bouguer gravity field by (1/wavelength) which tends to enhance the shorter wavelengths and, hence, the near surface content of the map. Note that bad data points are also strongly enhanced because they are represented by the very shortest wavelengths in the Fourier transformed domain.

This map displays many long linear features some of which are the near surface expressions of tectonic features such as faults and plate tectonic boundaries.

6. Second Vertical Derivative of Bouguer Anomalies

The second vertical derivative of the Bouguer anomaly field was calculated using Hildenbrand's Fourier transform filtering program. The effect of this filter is to multiply the various wavelength components of the Bouguer gravity field by $(1/\text{wavelength})^2$ which greatly enhances the shorter wavelengths and, hence, the near-surface density contrasts. The zero level of the second vertical derivative marks the steepest portions of anomalies and is frequently taken as a good indicator of the position of density boundaries and the horizontal limits of geologic bodies.

Because this filter greatly enhances the high frequencies--including those associated with bad data points--the data were initially upward continued to an elevation of 5 km before applying the second derivative filter in order to smooth some of the irregularities in the data. This is a compromise between noise and resolution.

7. Horizontal Gradient of the Bouguer Gravity

The magnitude of the horizontal gradient of the Bouguer anomaly field was calculated using the basic equation:

$$\left|\text{gradient}\right| = \sqrt{\left(\frac{\partial z}{\partial x}\right)^2 + \left(\frac{\partial z}{\partial y}\right)^2}$$

and the approximations that

$$\left(\frac{\partial z}{\partial x}\right)_{i,j} = \frac{z_{i+1,j} - z_{i-1,j}}{2(\Delta x)}, \text{ and } \left(\frac{\partial z}{\partial y}\right)_{i,j} = \frac{z_{i,j+1} - z_{i,j-1}}{2(\Delta y)}$$

This approximation can be shown to be equivalent to fitting a parabola at grid point i using z_i and its 2 neighboring values z_{i+1}, z_{i-1} and then calculating the slope of the parabola at i. The magnitude of the gradient of an anomaly depends on both the size of the density contrast and the nearness of the source to the surface. The largest gradients will occur nearly over the mass contrast in the case of anomalies produced by edges of geologic bodies. Cordell (1979) has used the horizontal gradient to locate faults. Many of the straighter gradients on this map are thought to mark major faults and structural boundaries of plate tectonic significance.

Horizontal gradients produced by linear anomalies are steepest over the two edges and gentle or flat along the tops of the anomalies so that there are two flanking high gradients (red) and a medial low gradient (blue). Nearly circular anomalies have their highest gradients going around them. The result on the color map is a red doughnut encircling the anomaly.

McGinnis and Ervin (1974), Long (1976), Forsyth (1977), and Simmons and others (1978) have pointed out apparent correlations of earthquakes with the gradient of the Bouguer gravity field. Although many earthquakes lie in areas with high gradients, there are also many large gradients which do not show signs of seismicity.

Perhaps the gradients with little associated seismicity mark structures which are not being reactivated since they are not favorably oriented with respect to the regional stress field. Another possibility is that our earthquake record is not long enough to establish the true patterns of seismicity.

It does appear that areas with low gravity gradients have fewer earthquakes. This may reflect a smaller number of major structures in these areas, but it is also possible that the lower gradients reflect a greater depth to the Precambriam basement which contains the structures under a thick cover of Paleozoic sedimentary rocks. If the Precambrian basement is deeper, it may be in a rheological regime where creep or plastic deformation is more likely to occur than brittle, earthquake-producing fracture.

8. Load Induced Stress Difference at 10 km

Topographic features and short wavelength masses producing anomalies must be supported to some extent by stresses in the crust (McNutt, 1980). To obtain an estimate of the magnitude and distribution of these stresses, the free air anomaly was converted to an equivalent two-dimensional density distribution which was then spread over the free surface of a semi-infinite elastic half-space. Ignoring the rather small terrain corrections for this region, this is equivalent to loading an elastic half-space with a surface load determined by the mass of the topographic features and then adding a second surface load determined as the equivalent 2D surface mass distribution which would produce the observed Bouguer anomalies. (Any gravity anomaly field can be accounted for in terms of a fictional "equivalent source" or "density coating" spread over a flat surface of observation (Grant and West, 1965, p. 214).)

The density contrasts, as represented by the equivalent surface sources, are more smeared than the actual sources at depth so that the stresses calculated will necessarily be more distributed and less concentrated than those actually occurring. The effect of loading all crustal mass anomalies at the surface rather than at their true depths also has the effect of increasing the stresses near the surface, but decreasing them at the depths at which the true sources lie. Both these effects will therefore probably tend to underestimate the load induced stresses at depth. However, for a first approximation, the computational simplicity of this approach has much to recommend it.

Another problem is that the elastic half-space assumption is a good approximation only for wavelengths shorter than the thickness of the earth's elastic layer--for wavelengths longer than this thickness, a more appropriate model would be an elastic layer over a plastic half-space of appropriate rheology. (In this map, unlike the corresponding map for the Northeast, the free air anomalies were not high pass filtered with a cutoff at 100 km.)

The surface load, inferred from the free air anomaly field, was then Fourier transformed to resolve its contribution into discrete wavelengths. The solution for a doubly sinusoidal load on an elastic half-space (Fung, 1965, p. 195) allows the stress tensor at any depth to be found by calculating the contribution from each separate wavelength and summing (doing the inverse Fourier transform).

The stress difference plotted on the map is the difference between the largest and smallest eigenvalues of the stress tensor calculated at a depth of 10 km. The stress difference serves as a crude measure of how close the homogeneous elastic material is to failure. It is our feeling that the stresses are, if anything, underestimated because of the various assumptions made.

In attempting to correlate the load induced stress difference with earthquake occurrence, another important variable is the mechanical heterogeneity of the crust. Although stresses presumably cause earthquakes, the vastly different mechanical properties of various rock types under various conditions of pressure and temperature may be at least as important as the concentration of large stresses in localizing earthquakes. In fact, the load induced stresses as calculated by this method correlate poorly with the general pattern of seismicity. The load induced stresses may well add on to other stresses to produce seismicity in some areas (Goodacre and Hasegawa, 1980), but in general they do not seem to be a primary cause of seismicity.

9. Terrain

The elevation data at 1' intervals were used to prepare this grid. The data were projected (Albers) and regridded to 2.032 km interval to give a scale of 1:2,500,000 on the color plotter.

10. Terrain Slope

The same process used to calculate the horizontal gradient of the Bouguer anomaly field was used to calculate the terrain slope.

REFERENCES CITED

Briggs, I. C., 1974, Machine contouring using minimum curvature: Geophysics, v. 39, p. 39-48.

Cordell, Lindrith, 1979, Gravimetric expression of graben faulting in Santa Fe Country and the Espanola Basin, New Mexico: New Mexico Geol. Soc. Guidebook, 30th Field Conf., Santa Fe Country, p. 59-64.

Forsyth, D. A., 1977, Reltionships between seismicity, free air gravity and structure in Arctic and eatern Canada (abs.): Earthquake Notes, v. 48, p. 15.

Fung, Y. C., 1965, Foundations of Solid Mechanics, Prentice Hall, Englewood Cliffs, N.J.

Goodacre, A. K. and Hasegawa, H. S., 1980, Gravitationally induced stresses at structural boundaries: Canadian Journal of Earth Sciences, v. 17, p. 1286-1291.

Grant, F. S., and West, G. F., 1965, Interpretation theory in applied geophysics: McGraw-Hill Book Company, N.Y., 584 p.

Hildenbrand, T. G., 1979, Preliminary documentation of program FFTFIL: U.S. Geological Survey, unpublished documentation.

International Association of Geodesy, 1971, Geodetic Reference System 1967: International Association of Geodesy Special Publication, no. 3, 116 p.

Long, L. T., 1976, Speculations concerning Southeastern earthquakes, mafic intrusions, gravity anomalies, and stress amplification: Earthquake Notes, v. 47, p. 29-35.

McGinnis, L. D., and Ervin, C. P., 1974, Earthquakes and block tectonics in the Illinois Basin: Geology, v. 2, 517-519.

McNutt, Marcia, 1980, Implications of regional gravity for state of stress in the Earth's crust and upper mantle: Journal of Geophysical Research, v. 85, p. 6377-6396.

Morelli, C., (ed.), 1974, The International Gravity Standardization Net 1971: International Association of Geodesy Special Publication, no. 4, 194 p.

Plouff, D., 1977, Preliminary documentation for a FORTRAN program to compute gravity terrain corrections based on topography digitized on a geographic grid: U.S. Geological Survey Open-File Report 77-534, 45 p.

Simmons, G., Tillson, D., Murphy, V., LeBlanc, G., Doherty, J., Sharp, J., and Roeloff, E., 1978, Gravity, stress, and earthquakes in Washington State and surrounding areas (abs.): 3rd International Conference on Basement Tectonics, 15-19 May 1978, Fort Lewis College, Darango, CO.

Simpson, R. W., Bothner, W. A., and Godson, R. H., 1981, Colored gravity anomaly and terrain maps of the Northeastern U.S. and Adjacent Canada: U.S. Geological Survey Open-File Report 81-560.

Ulrych, T. J., 1968, Effect of wavelength filtering on the shape of the residual anomaly: Geophysics, v. 33, p. 1015-1018.

Webring, M. W., 1977, Preliminary documentation--gridding program MINC: U.S. Geological Survey unpublished documentation.

Zoback, M. L., and Zoback, M. D., 1980, State of stress in the conterminous United States: Journal of Geophysical Research, v. 85, p. 6113-6156.

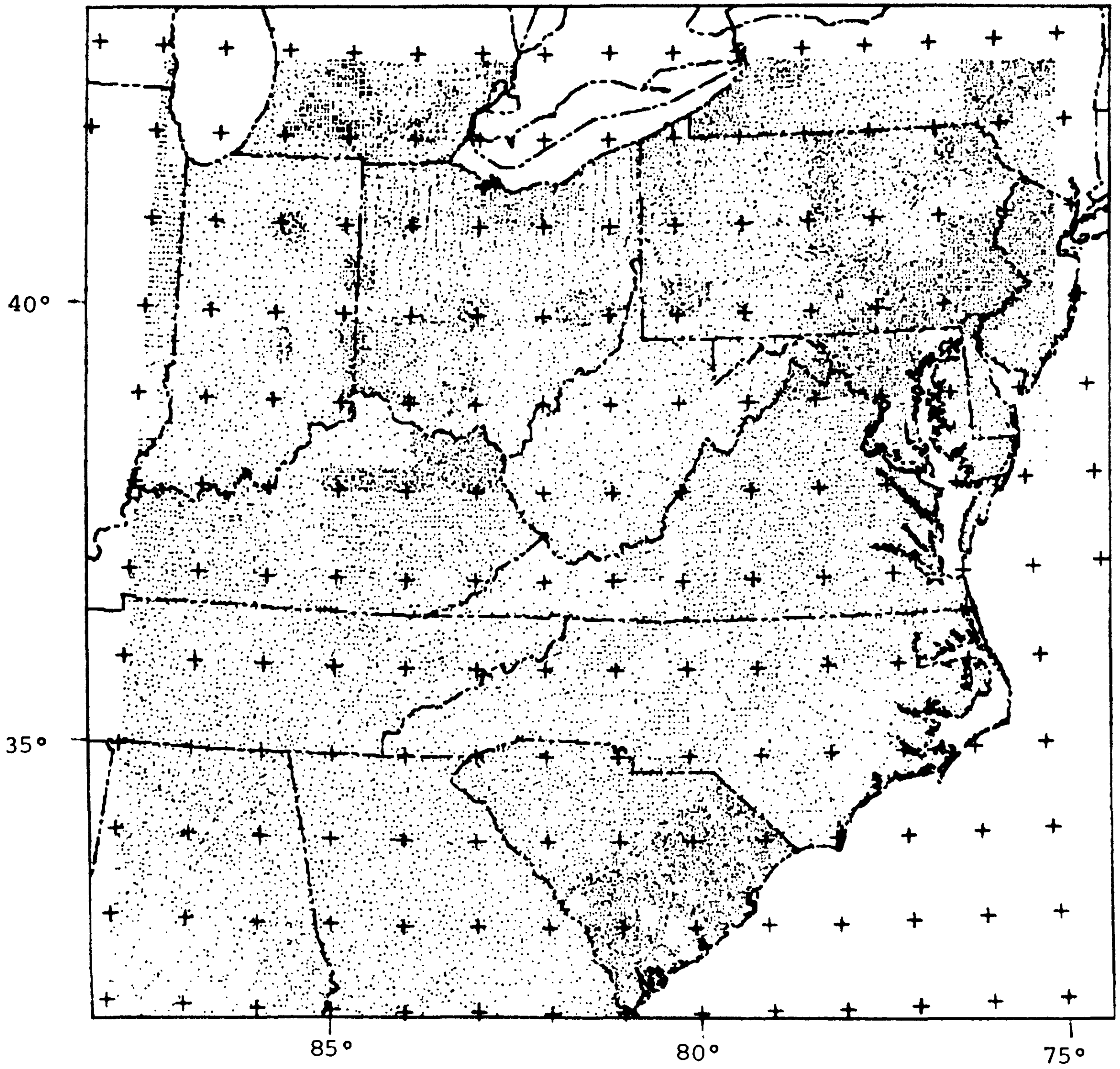

Figure 1. Data set screened at approximately 6 km.

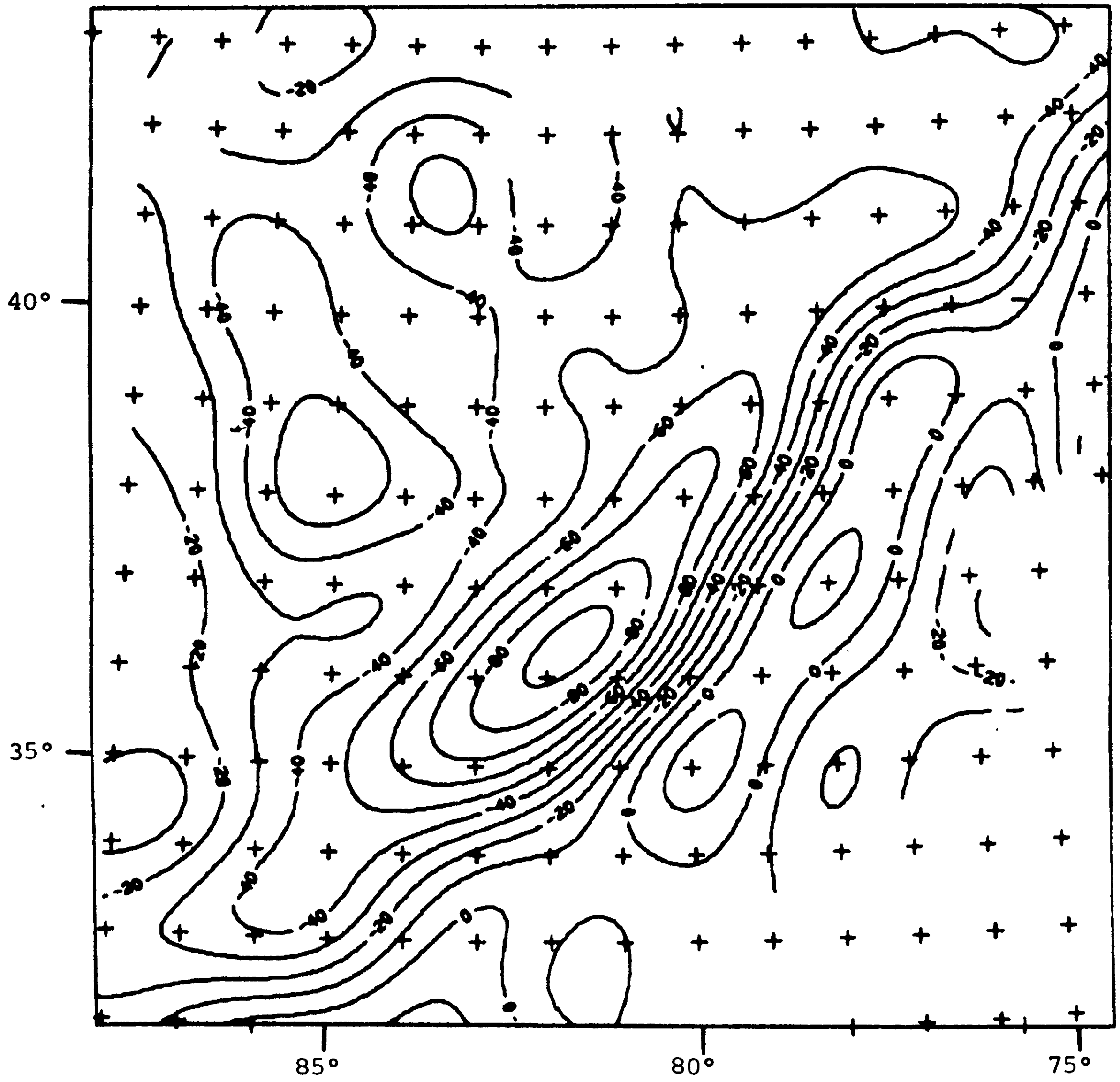

Figure 2. Regional Bouguer Anomaly field composed of wavelengths greater than 250 km.

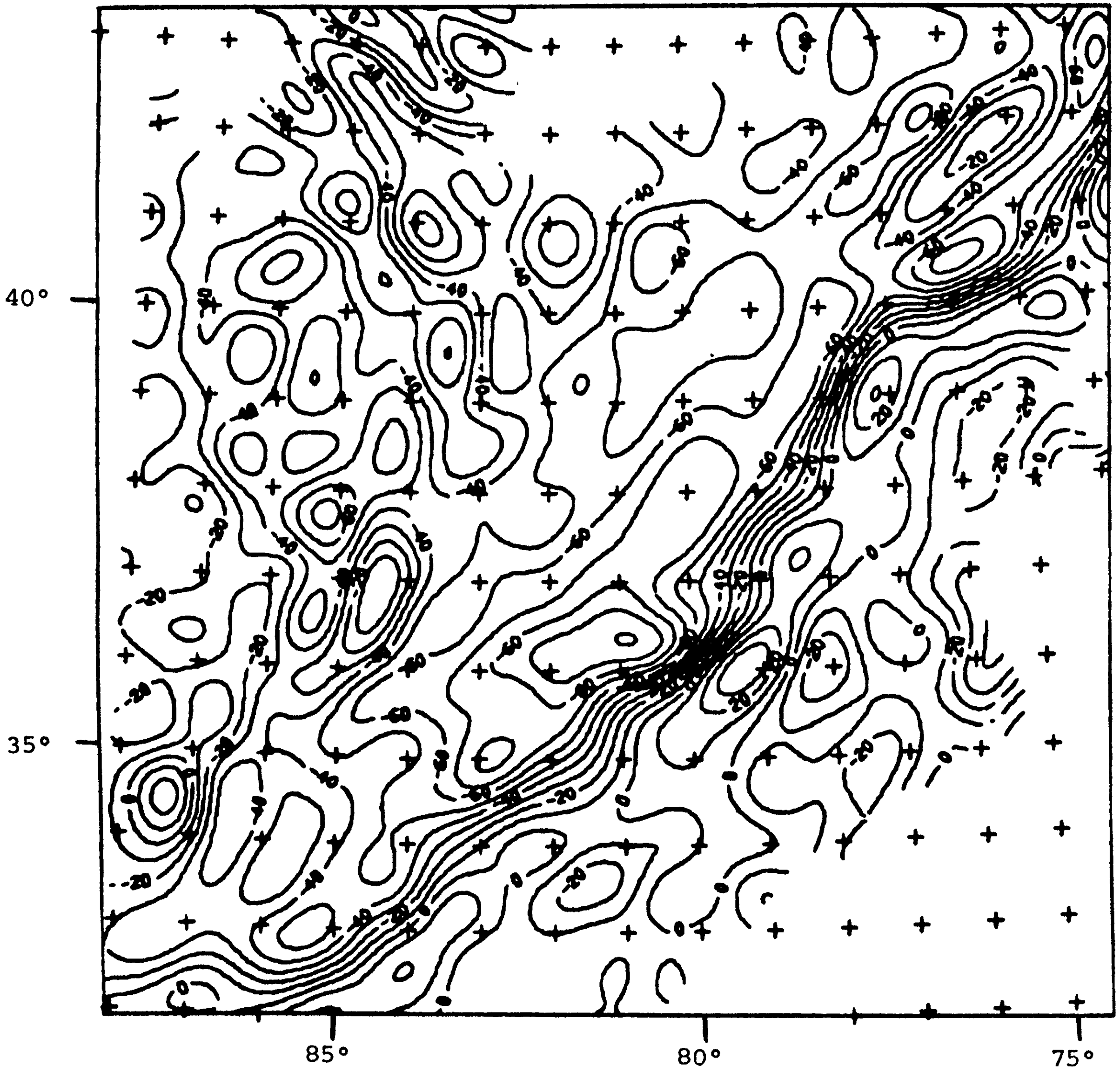

Figure 3. Regional Bouguer Anomaly Field composed of wavelengths greater than 100 km.

MAP 1. Free Air Gravity (range = -60 to +50 milligals)

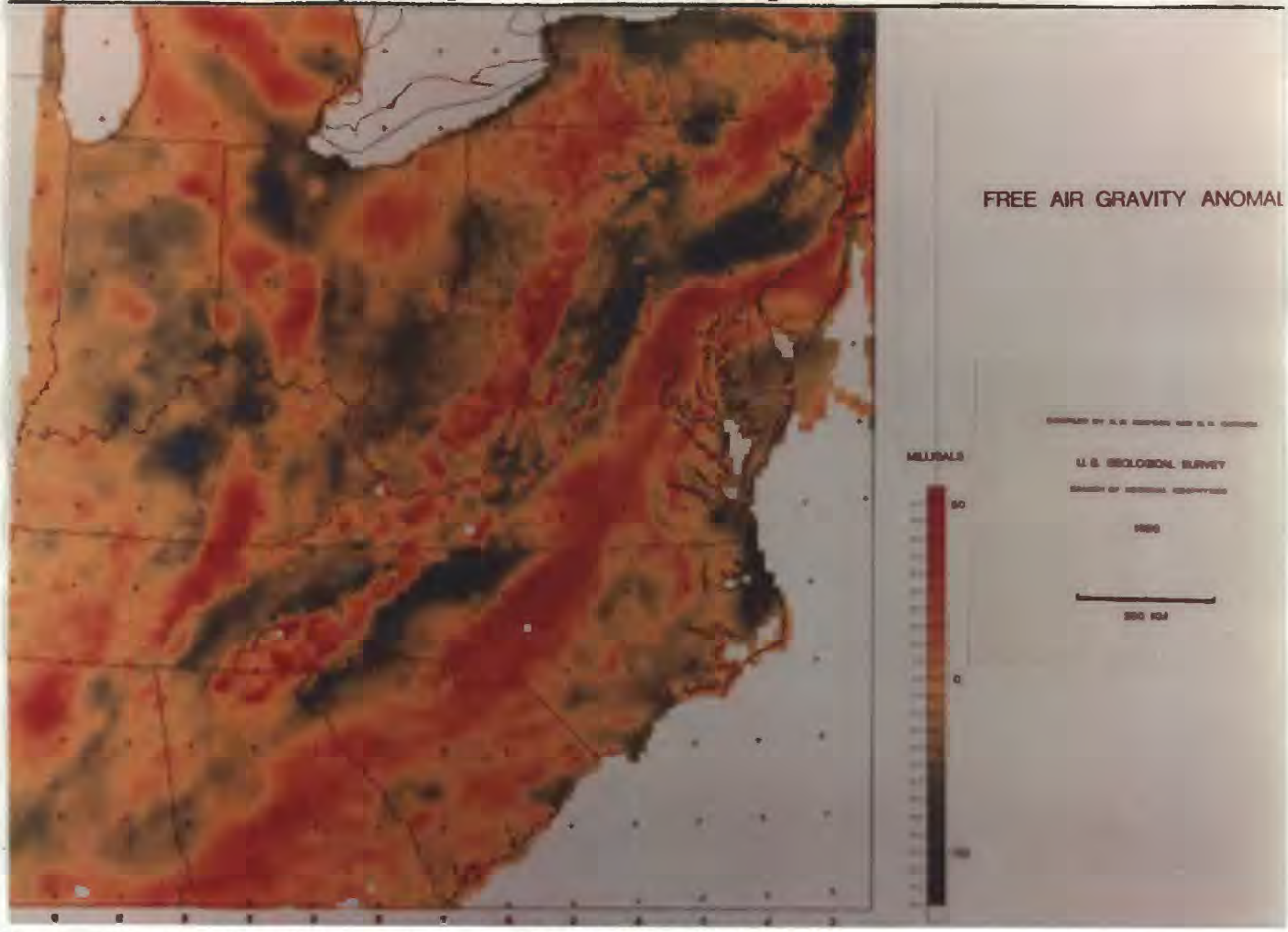

MAP 2. Bouguer Gravity (range = -95 to +30 milligals)

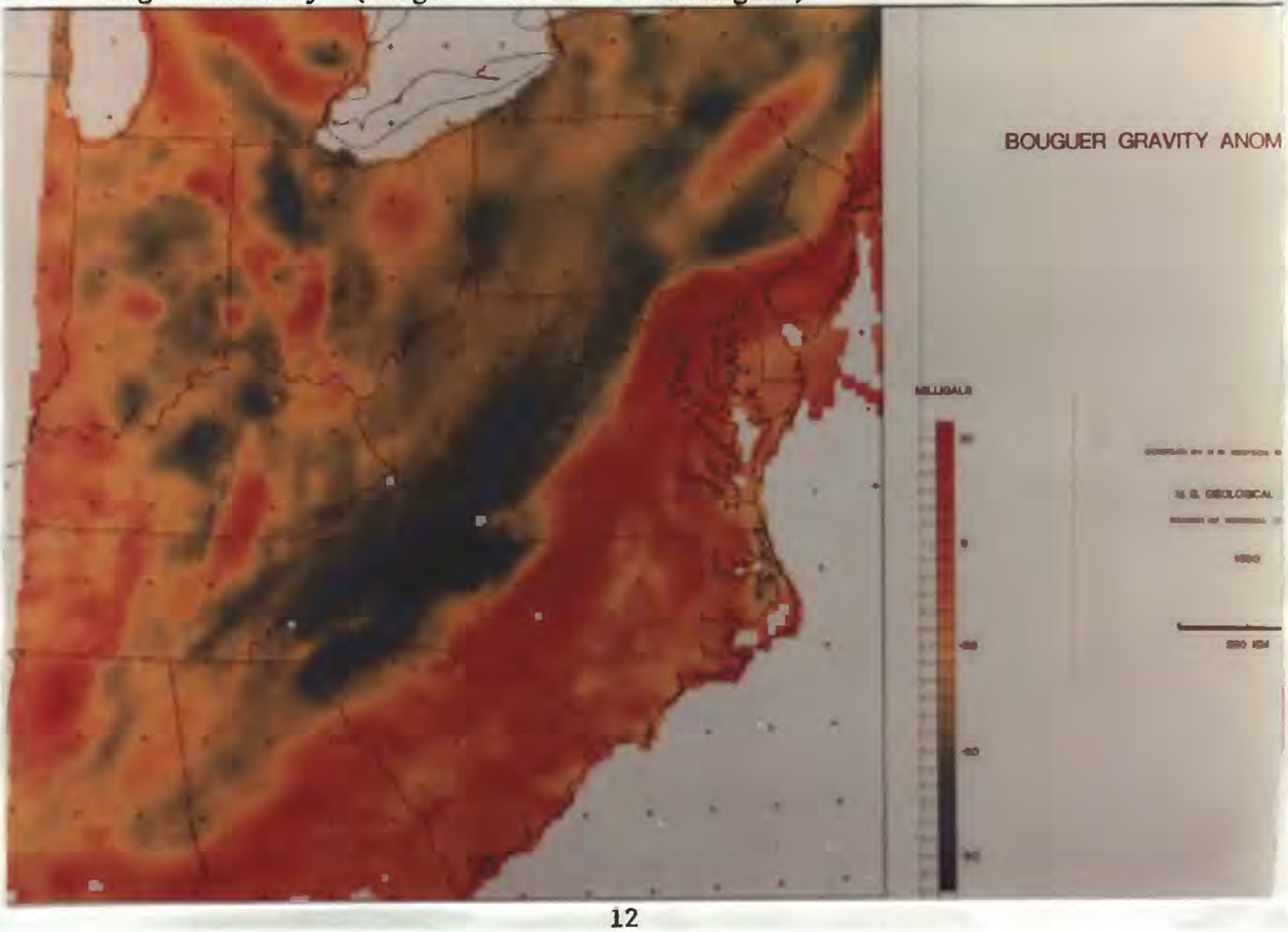

MAP 3. Bouguer Residual, 250km (range = -30 to +30 milligals)

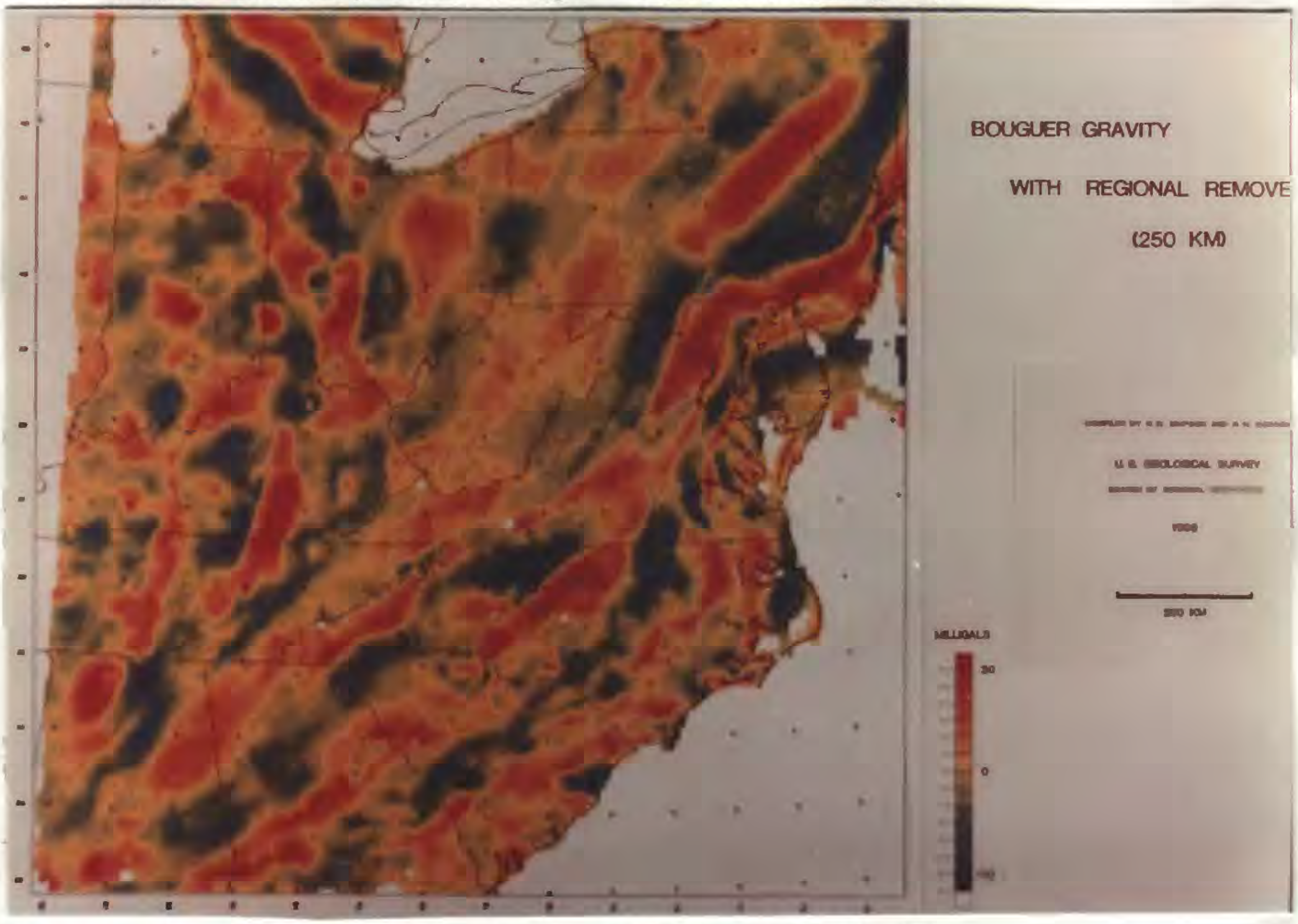

MAP 4. Bouguer Residual, 100km (range = -30 to +30 milligals)

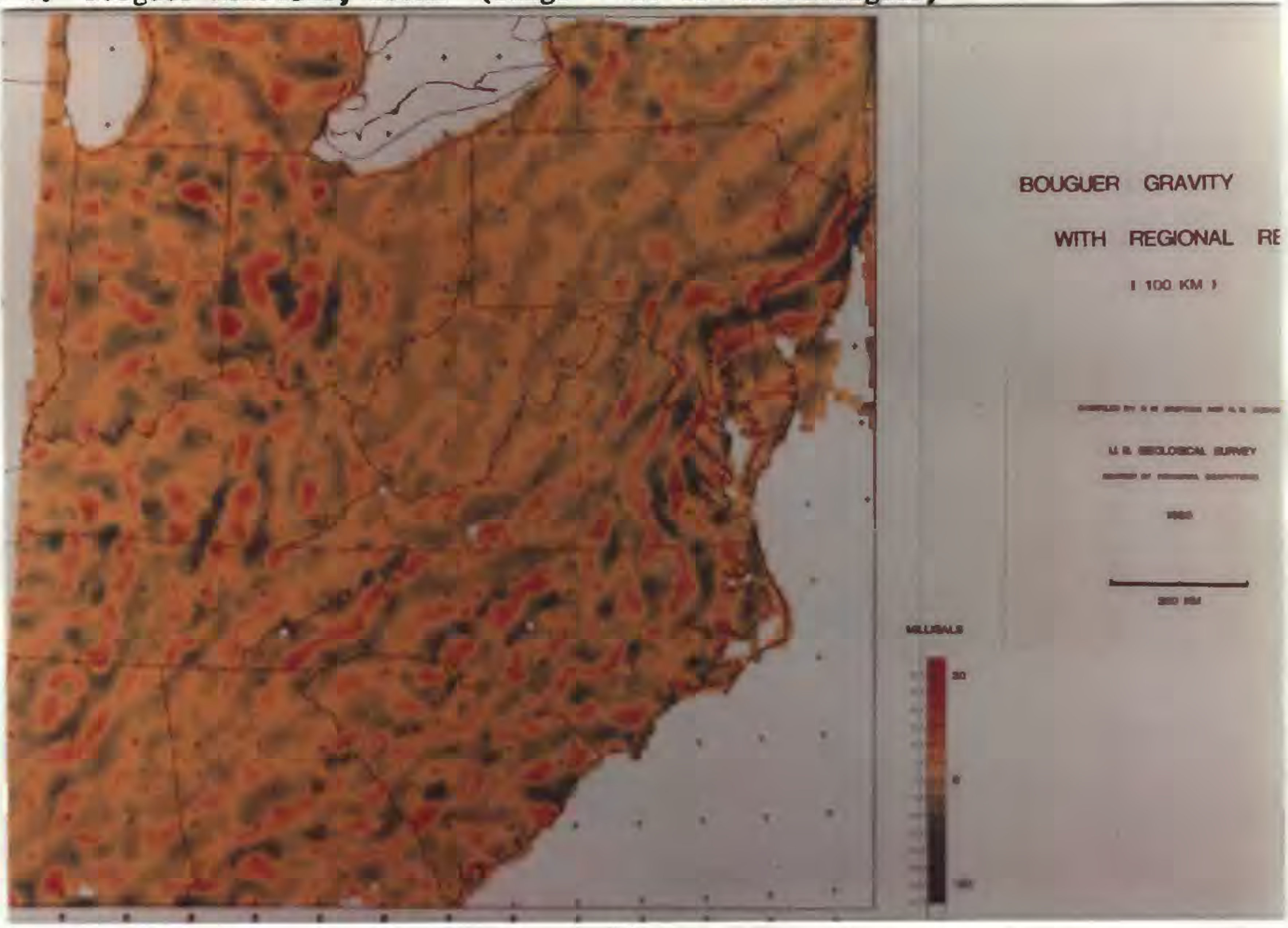

MAP 5. First Vertical Derivative (range = -4.5 to +4.5 milligals /km)

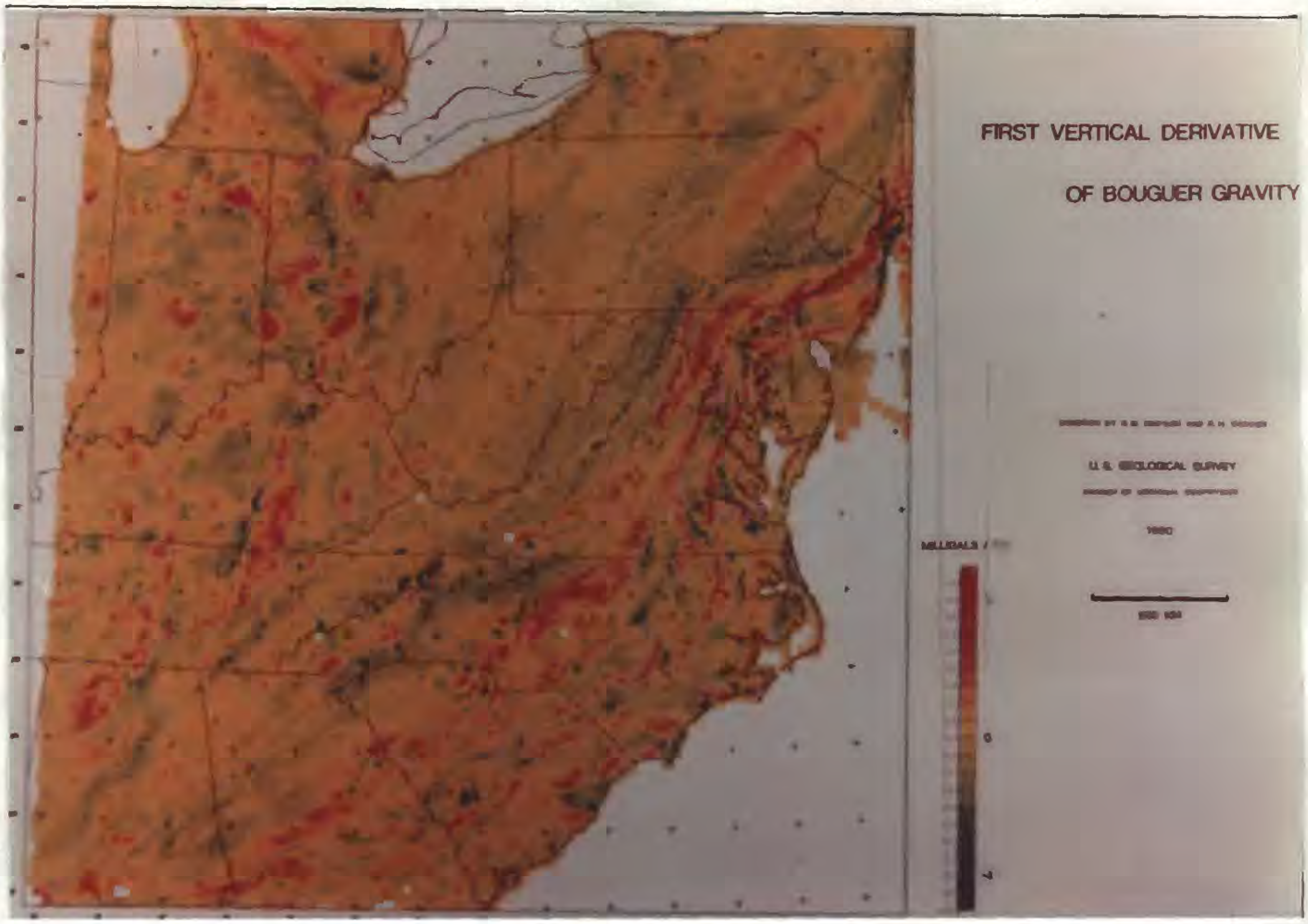

MAP 6. Second Vertical Derivative (range = -0.3 to +0.3 milligals/km^2)

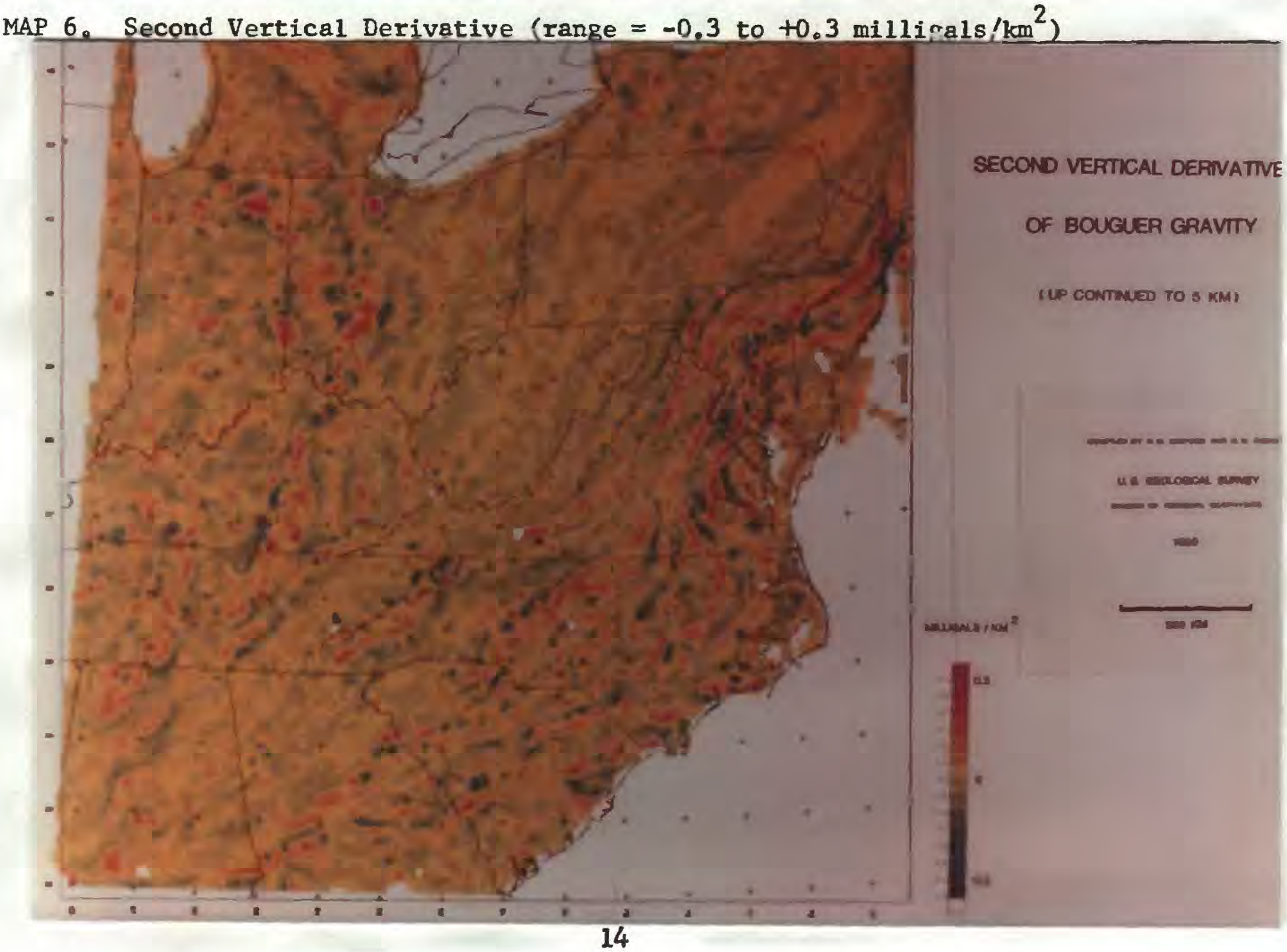

MAP 7. Horizontal Gradient of Bouguer Gravity (range = 0 to 2.0 milligals/km)

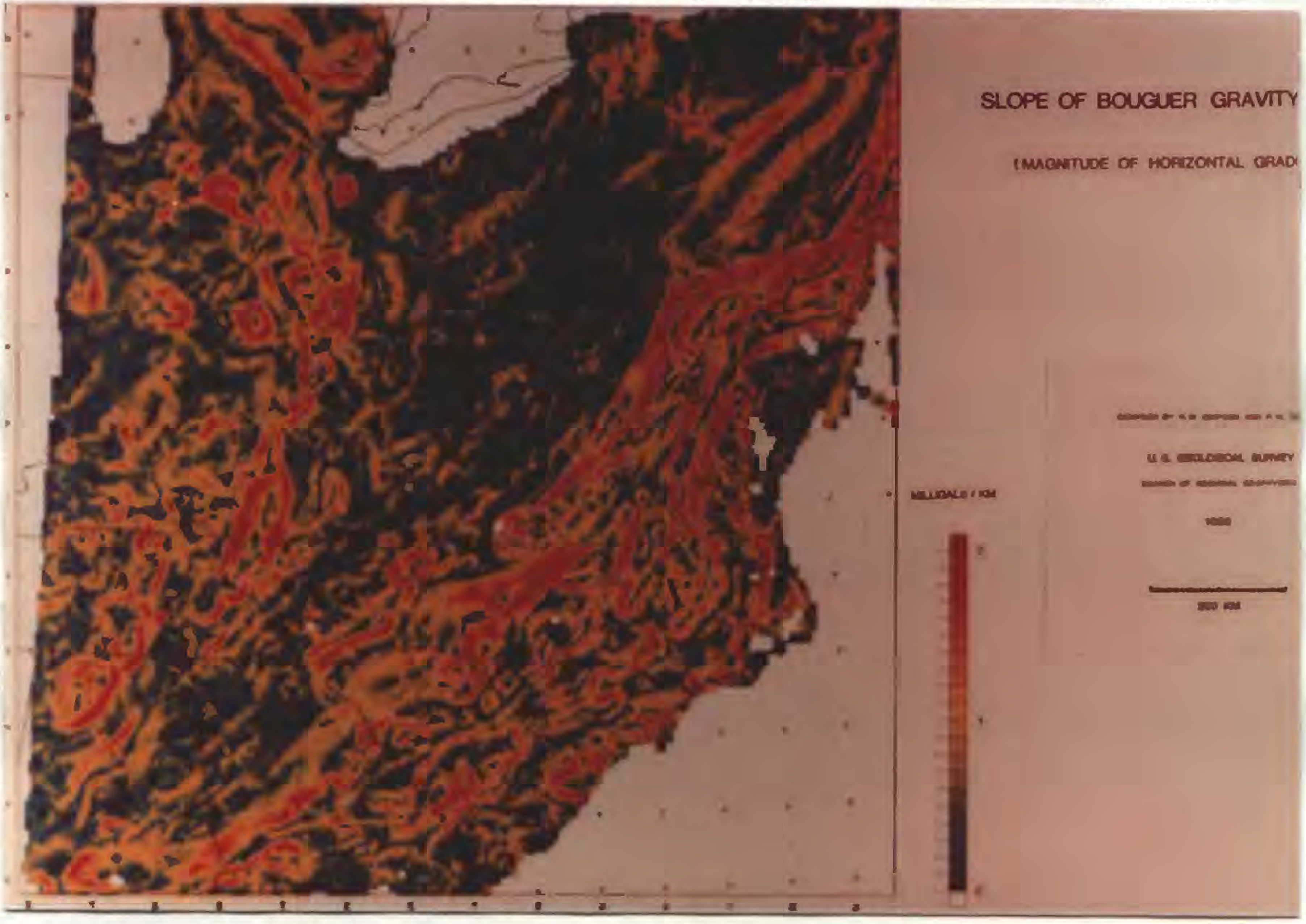

MAP 8. Load Induced Stress Difference at 10 km (range = 0 to 80 bars)

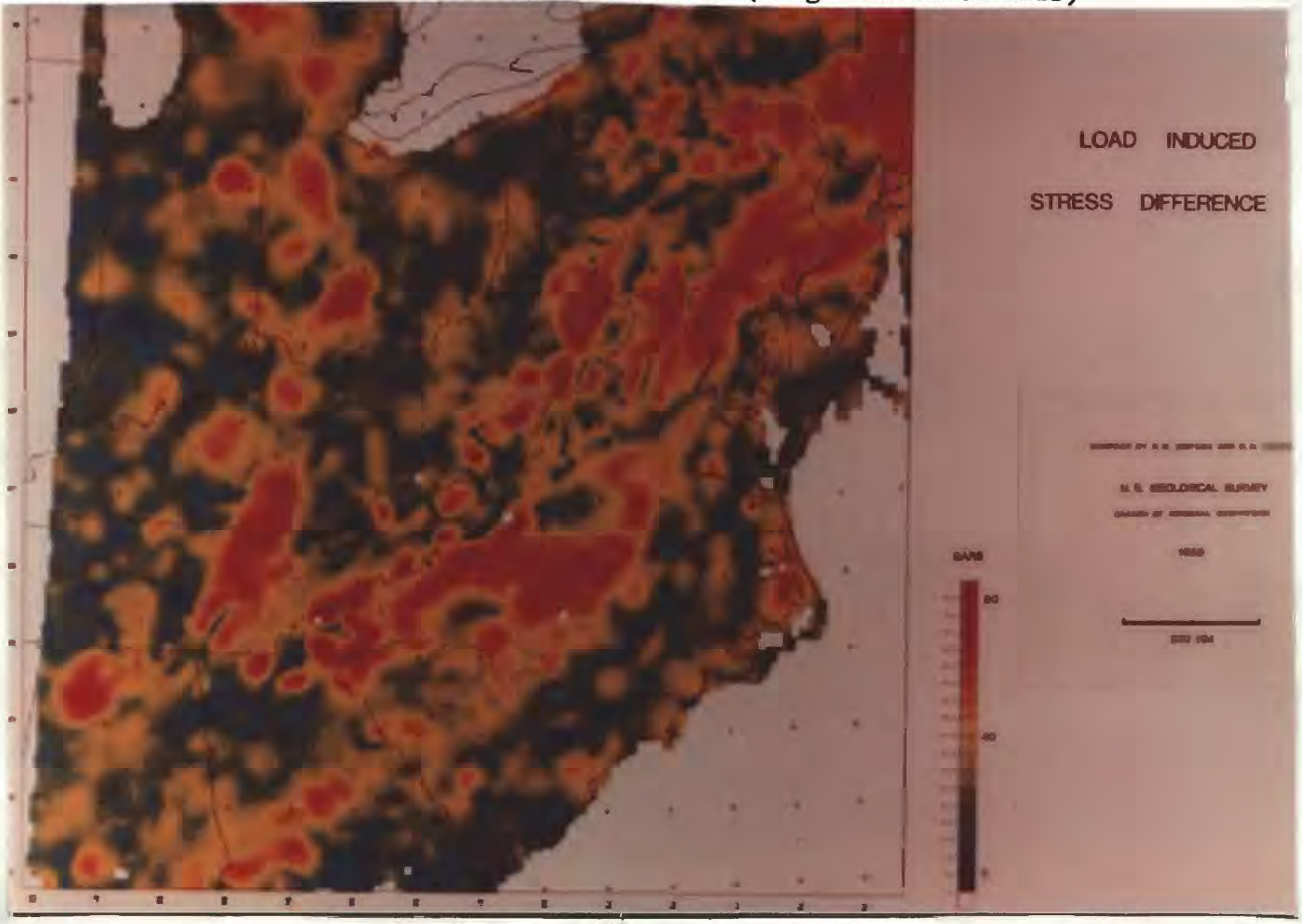

MAP 9. Terrain (range = 0 to 1550 meters)

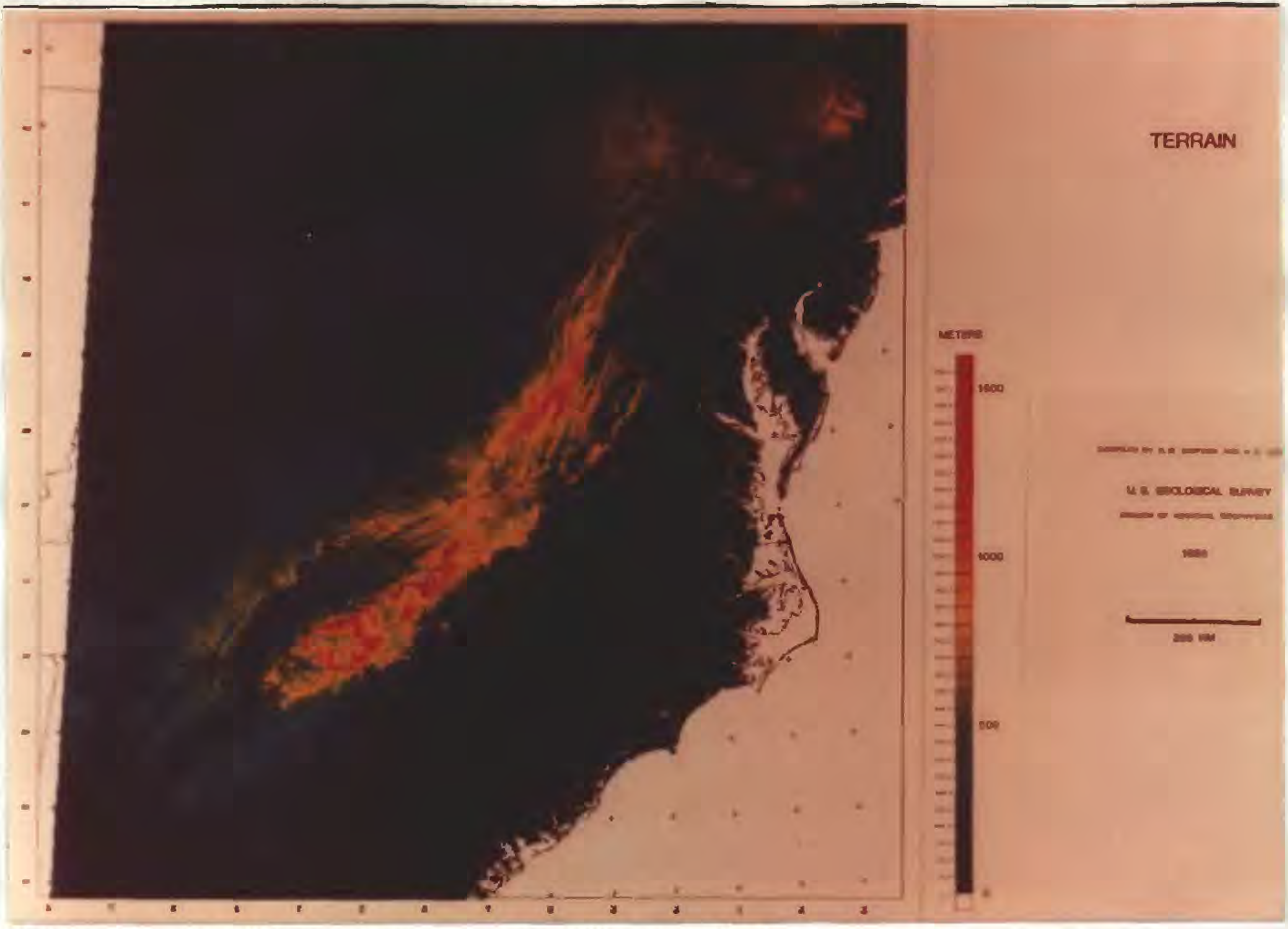

MAP 10. Terrain Slope (range = 0 to 100 meters/km)